Journal of Catalysis 320 (2014) 89–96

Contents lists available at ScienceDirect

Journal of Catalysis

journal homepage: www.elsevier.com/locate/jcat

Controlling CH_2 dissociation on Ru(0001) through surface site blocking by adsorbed hydrogen

Harald Kirsch [1], Xunhua Zhao [1], Zefeng Ren [2], Sergey V. Levchenko, Martin Wolf, R. Kramer Campen *

Fritz Haber Institute of the Max Planck Society, 4-6 Faradayweg, 14195 Berlin, Germany

ARTICLE INFO

Article history:
Received 28 July 2014
Revised 26 September 2014
Accepted 28 September 2014
Available online 27 October 2014

Keywords:
Methane dissociation
Methane coupling
Density functional theory
Sum frequency generation

ABSTRACT

Understanding the relative stability of CH_x species on surfaces is necessary for mechanistic description of much important catalytic chemistry. Here, we experimentally quantify the barrier of the reaction $CH_2 \rightarrow CH + H$ on Ru(0001) in UHV and find an activation energy, 65 ± 6 kJ/mol, that is >4× higher than previous computational results with 0, 1, or 2 coadsorbed H atoms per CH_2, *i.e.* 16 kJ/mol. Employing density functional theory calculations, we show that this disagreement can be reconciled if 3 coadsorbed H atoms per CH_2 are present in our experiment. We further demonstrate, by calculating the surface phase diagram for one carbon species on Ru(0001) as a function of H_2 chemical potential, that the additional hydrogen surface coverage requires non-equilibrium conditions. Such conditions may be important at the high temperatures and pressures of real catalytic systems.

1. Introduction

The heterogeneous chemistry of one carbon (C_1) compounds on transition metal surfaces is important for such applications as the steam reforming of methane (overall reaction $CH_4 + H_2O \leftrightarrow CO + 2H_2$) and the Fischer–Tropsch synthesis (in which $CO + H_2$ react to form longer chain hydrocarbons) [1–6]. Much prior work has illustrated that for both these processes, the relative stability of surface-bound CH_x radicals is of paramount importance.

In the Fischer–Tropsch process in particular, while several decades of work have clarified that long chain hydrocarbon growth happens via addition of reduced C_1 compounds, identification of the most important C_1 compound for this process has proven challenging. While both product distributions and isotope studies at various transition metal (*e.g.* Cobalt, Ruthenium, and Iron) surfaces suggest that adsorbed CH_2 radicals play an important role [7,8], other experiments as well as theory find this species unstable and suggest chain growth mechanisms in which adsorbed CH radicals or C are the fundamental building blocks [6].

From the steam-reforming perspective, it is clear that methane dehydrogenation and adsorption of CH_3 radicals is the necessary first step; however, the details of the subsequent chemistry are strongly dependent on the relative stabilities and reactivities of CH_3, CH_2, CH, and C on a particular transition metal for a particular surface structure. Thus, for both processes, the thermodynamics and kinetics of the $CH_2 \rightarrow CH$ reaction are of importance.

In engineered applications such hydrocarbon chemistry is usually performed in high surface area transition metal fixed bed reactors at high temperatures and pressures. Because of catalyst structural heterogeneity and possible mass transport limitations these systems make elucidation of the fundamental reactions that underlie these processes challenging. To gain mechanistic, molecular-level insights of the sort described above, much attention has focussed on appropriate model systems: in particular the adsorption of methane, its dehydrogenation and the (possible) coupling of the resulting C_1 radicals on a variety of single crystal transition metal surfaces (*e.g.* Ni, Ru, Rh, and Co) under ultra-high vacuum (UHV) conditions [9,10,2–5]. This approach has the benefit of minimizing structural heterogeneity and allowing the straightforward preparation of clean samples. Because of its high thermal stability and high reactivity, ruthenium single crystals, particularly the Ru(0001) surface, have become a favorite for the investigation of C_1 surface chemistry.

While thus clearly scientifically important, the study of methane adsorption and dehydrogenation on Ru(0001) in UHV affords several practical experimental challenges. Chief among them is that the initial sticking probability of CH_4 on Ru(0001) decreases from

* Corresponding author.
E-mail addresses: kirsch85@fhi-berlin.mpg.de (H. Kirsch), xunhuazhao@fhi-berlin.mpg.de (X. Zhao), zfren@pku.edu.cn (Z. Ren), levchenko@fhi-berlin.mpg.de (S.V. Levchenko), wolf@fhi-berlin.mpg.de (M. Wolf), campen@fhi-berlin.mpg.de (R.K. Campen).

[1] HK and XZ contributed equally to this work.

[2] Present address: International Center for Quantum Materials and School of Physics, Peking University, No. 209 Chengfu Road, 100871 Beijing, China.

http://dx.doi.org/10.1016/j.jcat.2014.09.023
0021-9517/

10^{-7} to 10^{-9} on lowering sample temperatures from 550 K to 400 K [9,11], thus making dissociative adsorption of CH_4 essentially impossible below 400 K in UHV. Prior workers have typically overcome this challenge by the use of a high-pressure cell to enhance dissociative adsorption (and then transfer of the sample to UHV for characterization), but even using this approach, studying CH_4 adsorption at sample temperatures under ≈350 K has proven extremely difficult. Characterization of samples prepared in this manner at these temperatures via electron energy loss spectroscopy (EELS) suggests significant concentration of C, CH or two-carbon compounds, but essentially no CH_3 or CH_2 groups [12,13].

One way to rationalize these experimental trends is that single crystal surfaces prepared in this manner sample the equilibrium distribution of hydrocarbon products at the elevated temperature at which they are prepared, and that the thermal stability of CH_3 and CH_2 is significantly lower than other C_1 species. Indeed, experiments that directly produce CH_3 radicals on Ru(0001) are consistent with this picture. Zhou and coworkers have shown that by dosing Ru(0001) with CH_3I via a partial pressure increase of 1×10^{-10} mb at sample temperatures below 200 K, one can generate adsorbed CH_3 radicals [14]. With increasing temperature, they find CH_3 converted to CH_2 and subsequently to CH: between 250 and 300 K virtually all CH_2 is converted to CH. Kiss and coworkers [15,16] observed a comparable thermal stability for CH_2 in the reaction of CH_2I_2 on Ru(0001). Prior theoretical work is consistent with this relative instability of CH_2. Van Santen and coworkers [17] have shown that the barrier for the $CH_2 + xH \rightarrow CH + (x+1)H$ reaction is ≈16 kJ/mol in the presence of 0, 1, or 2 coadsorbed hydrogen atoms per 2×2 surface unit cell. Moreover, in the same study, they predicted that the barrier for the $CH \rightarrow C$ reaction is substantial, 110 kJ/mol, a result confirmed experimentally [18].

While the relative stabilities of CH_2 and CH on Ru(0001) seem clear understanding the molecular mechanism of this stability, and therefore the connection of these results to real catalytic systems remains quite challenging. The crucial issue here is that experimental studies in which CH_4 is dosed on Ru(0001) have largely focussed on the samples created at high temperatures and pressures and analyzed in UHV. Even assuming such samples reach thermal equilibrium during dosing, it is difficult to know how the transfer to UHV may affect surface speciation. Similarly, computational/theoretical work has largely focussed either on samples at thermal equilibrium with the adjoining gas phase or on samples with relatively low surface coverages of carbon and hydrogen, and so have investigated the thermodynamics and kinetics of interconversion of one or two carbon compounds in the absence of high (and presumably non-equilibrium) surface coverages of either carbon or hydrogen.

Further complicating any attempt to connect the results of these catalytic model systems with real reactors, such systems must be either ender- or exergonic, *i.e.*, not at equilibrium. A microscopic picture seems in accord with this macroscopic departure from equilibrium, the significant surface structural heterogeneity in such reactors would require equilibrium between *all* carbon-containing species at *all* surface sites, a scenario inconsistent with, for example, the slow (hours to years) poisoning of catalyst surfaces by coke formation.

In this study, we employ a supersonic molecular beam source to dose the Ru(0001) surface with methane at temperatures below 250 K. As we will show, employing such a source at these sample temperatures allows the preparation of surface-bound CH_2 radicals from CH_4 without leaving UHV. Because at such temperatures atomic H is stable on the Ru(0001) surface [19], this approach further allows us to understand the effect of non-thermal distributions of surface hydrogen. Having prepared such a sample, we characterize the surface population of CH_2 after annealing it to successively higher temperatures using the surface-specific laser-based technique, vibrational sum frequency spectroscopy. By conducting a series of such experiments as a function of sample annealing temperature, we extract the activation energy (E_a) for conversion of $CH_2 \rightarrow CH$. We find a value of 65 kJ/mol, ≈4× higher than previous estimates by theory.

To provide a microscopic understanding of this experimental observable, we calculate adsorption energies of all relevant C_1 species, the reaction pathways and transition states for CH_2 to CH conversion, and the phase diagram of the CH_4/Ru(0001) system as a function of hydrogen chemical potential, using the *ab initio* atomistic thermodynamics approach [20]. The results of these calculations demonstrate that, above a critical threshold of hydrogen surface coverage of Ru(0001) terraces, the relative stability of CH_2 and CH is substantially modified, and the barrier for $CH_2 \rightarrow CH$ conversion increases dramatically, in agreement with our experiments. Interestingly, these high coverages of CH_2 and coadsorbed H atoms are found to be energetically unfavorable if surface hydrogen is in equilibrium with gas-phase H_2 at any chemical potential. Evidently, non-equilibrium distributions of coadsorbed hydrogen dramatically change CH_2 reactivity on Ru(0001). The dependence of CH_2 stability on coadsorbed hydrogen that we observe provides a possible means of reconciling experiment and computation describing the C_1 building block in the Fischer–Tropsch process and, more generally, suggests the importance of understanding surface concentrations of hydrogen in the heterogeneous chemistry of hydrocarbon conversion.

2. Methods

2.1. Experimental

The experiments were performed in a UHV chamber, pumped by a turbo-molecular pump, with a base pressure of $1.5 \cdot 10^{-10}$ mbar. We overcome the temperature-dependent sticking coefficient of CH_4 on Ru(0001) [4] by dosing methane using a three-stage supersonic molecular beam source (MBS), modeled after prior workers [21,22]. As observed previously by others for methane dosing on other transition metal surfaces [5], the increased kinetic energy of each CH_4 molecule in this setup enhances the sticking coefficient of methane by $\approx 10^5$, enabling surface science investigation for surface temperatures (T_{Ru}) less than 300 K [9]. In our experiments, preparation of methane-derived surface radicals was performed by dosing 5% CH_4 seeded in Helium (Westphalen AG, Münster) with the MBS on a clean Ru(0001) surface. The temperature of the nozzle (T_{Nozzle}) was set for all measurements to 980 K, corresponding to a kinetic energy of approximately 0.75 eV for each CH_4. It has been reported that nozzle temperatures above 860 K induce partial dehydrogenation of methane in a similar setup [23]. Additionally, the CH_4/He mixture we employed was certified by the manufacturer to contain <0.5 ppm H_2. Given hydrogen from these two sources we estimate that we have a minimum of one H atom per 2×2 unit cell coadsorbed with each CH_4 molecule. The consequences of this hydrogen are explored in detail below, and a quantitative estimate of these fluxes is included in the Supporting Information.

Measurement of the Ru surface temperature, T_{Ru}, was performed using Chromel/Alumel thermocouples spot-welded to the side of the sample. The sample temperature was controlled by a Lakeshore temperature controller connected to a resistance heating/liquid N_2 cooling unit. Before each measurement, the Ru crystal (0001) surface was cleaned by 20 min Ar^+-sputtering (sputter current ≈5 μA), followed by a 10 min baking at 1260 K while exposed to 10^{-7} mbar O_2, followed by a final heating of the crystal to 1510 K. This procedure has been shown to produce a Ru(0001) surface free of both contaminants and damage [24].

For practical purposes, we wish to prepare a sample that has high numbers of surface CH_2 groups but low numbers of other types of carbon-containing surface species. This implies that we wish to keep T_{Ru} low enough so that thermal induced dissociation of CH_2 does not take place but high enough to allow appreciable dissociative adsorption of methane. As anticipated based on prior work [14–16], we found T_{Ru} = 250 K to best fulfill both these conditions. All data shown in this paper were thus collected from samples dosed at this temperature.

After sample preparation, T_{Ru} was lowered to 110 K for the spectroscopic characterization of the adsorbed species. At this T_{Ru}, control experiments (data not shown) show hydrocarbon surface speciation stable over days. After quantifying the spectral response of the *as created* sample, T_{Ru} is rapidly raised (using a temperature ramp of 100 K/min) to an indicated elevated temperature for five minutes. After these five minutes, the sample is once again cooled to 110 K, and an additional vibrational spectra collected. As will become clear below, this treatment clearly shows a CH_2 spectral response that decreases in intensity with increasing maximum temperature of the annealing/baking step. We wish to understand what this temperature dependence tells us about the barrier of the $CH_2 \rightarrow CH + H$ reaction (see Fig. 1 for a graphical depiction of the experimental approach).

For spectroscopic characterization of the sample, we employ the laser-based technique, vibrational sum frequency (VSF) spectroscopy. In a VSF measurement, the output of pulsed infrared and visible lasers is overlapped spatially and temporally at an interface, and the emission at the sum of the frequencies of the two incident fields is monitored. This sum frequency emission is, by its symmetry selection rules, interface-specific, and tuning the incident infrared (IR) light frequency in resonance with an interfacial mode creates a several order of magnitude increase in VSF emission (for background to the technique see [25–28]). The observed sum frequency intensity is a function of molecular orientation, beam incident angles and polarization and the product of the molecular polarizability and transition dipole squared. Our VSF approach has two technical advantages over Electron Energy Loss Spectroscopy (EELS) and Reflection Absorption Infrared Spectroscopy (RAIRS) measurements of this system: in contrast to EELS, it is relatively straightforward to achieve the spectral resolution necessary to distinguish all possible CH-containing intermediates, and in contrast to RAIRS, we detect visible (not infrared) photons and thus detection is substantially more sensitive [29].

For the VSF measurements, we employed a commercial Ti:sapphire laser system from Quantronix (Model Titan 7), that delivers 800 nm, 110 fs pulses with a pulse energy of 3.2 mJ at 400 Hz. Approximately 3 mJ of this output were used to pump an OPG/OPA (Optical Parametric Amplifier, TOPAS, Light Conversion) providing tunable, broadband IR pulses. For all experiments described here, the central wavelength of this IR source was set to 3.4 μm, the bandwidth 130 cm^{-1} at full-width half-maximum (FWHM), the energy per pulse 10–15 μJ, and the pulse duration ≈150 fs.

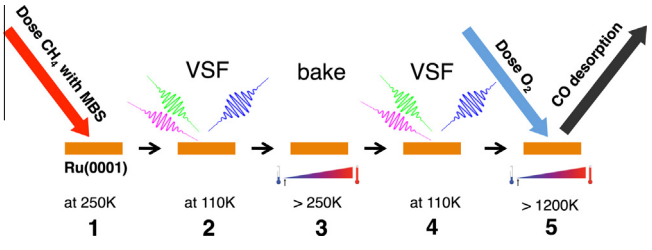

Fig. 1. Experimental scheme showing the dose-characterize-anneal-characterize cycle for a measurement of $CH_2 \rightarrow CH$ barrier as a function of annealing temperature.

The *visible* pulse in the VSF measurements was created by spectrally narrowing the remaining 800 nm energy from the OPA/OPG process using a homebuilt pulse shaper. After narrowing, 7–12 μJ of energy per pulse remain. To conduct a measurement, the IR and VIS pulses are focused on the sample surface, with incident angles of 75° and 70° relative to the surface normal, respectively. After generation on the sample, the dispersed VSF signal is collimated, filtered, focused onto a grating in a spectrometer (1800 g/mm), and dispersed across an ICCD detector (intensified charge-coupled device) for analysis. All data shown in this study were collected with all three fields polarized in the plane of incidence (*i.e.* p-polarized light for SFG/Vis/IR, called ppp-polarization).

As discussed above, when any frequency component of the broadband IR pulse matches that of a vibrational transition of an interfacial molecule, enhancement of the VSF emission will result. To quantify this vibrational response, we follow prior workers and model the VSF intensity (I_{VSF}) as a coherent superposition of a nonresonant background (in our case dominated by the metallic substrate) and homogeneously broadened resonances [30]:

$$I_{VSF} \propto \left|\chi^{(2)}_{eff}\right|^2 = \left|\chi^{(2)}_{NR} + \chi^{(2)}_{R}\right|^2 = \left||A_{NR}|\, e^{i\phi_{NR}} + \sum_q \frac{A_q}{\omega_{IR} - \omega_q + i\Gamma_q}\right|^2 \quad (1)$$

in which $\chi^{(2)}_{NR}$ is the nonresonant response, $\chi^{(2)}_{R}$ is the resonant response, A_q is the complex resonance amplitude, ω_q is the center frequency, and $2\Gamma_q$ is the line width of the q^{th} resonance, $|A_{NR}|$ is the nonresonant amplitude, and ϕ_{NR} is the nonresonant phase. While $\chi^{(2)}_{R}$ is a macroscopic quantity, it can be straightforwardly related to the molecular hyperpolarizability $\beta^{(2)}$ (assuming molecular orientation and beam incident angles and polarizations are constant),

$$\chi^{(2)}_{R} \propto N\beta^{(2)} \quad (2)$$

in which N is the number of molecules in the laser spot. All quantitative line shape analysis was done by fitting Eq. (1) to the data using the Levenberg–Marquardt algorithm as implemented in the analysis program Igor-Pro (Wavemetrics).

After finishing all VSF measurements of a particular sample, we quantified carbon surface coverage by temperature-programmed oxidation (TPO): we dose the surface with O_2 at 300 K and quantify the amount of CO that is emitted with increasing temperature using a Feulner cup quadrupole mass spectrometer(LM500, Specs). For higher carbon coverages, we repeat this dosing-heating cycle until no additional CO is emitted. Because the surface density of a monolayer of CO on Ru(0001) is well known ($1.58 \cdot 10^{19}$ sites per m^2 [9]), and because one monolayer of CO is known to correspond to 0.57 ML of adsorbed carbon [31,32], we can straightforwardly calibrate the amount of carbon present for each sample preparation. All samples used in this study had a surface coverage of 0.18 ± 0.02 of a ML of carbon.

2.2. Computational

Density functional theory [33,34] calculations were performed with the all-electron code FHI-aims, employing numerical atom-centered orbitals [35]. The Perdew-Burke-Ernzerhof (PBE) exchange–correlation functional [36], periodic models, and the default "tight" basis were used in all calculations in this work. Van der Waals interaction was included using a first-principles C_6/R^6 correction scheme with the C_6 coefficients re-scaled to account for the screening effects at the metal surface (the vdW^{surf} method [37]). The Ru(0001) surface is modeled by a seven-layer slab with two relaxed layers and five layers fixed at bulk geometry. Adsorbates were put only on the unconstrained

side of the slab. The vacuum distance between neighboring slabs is more than 35 Å to avoid interaction between slabs. We employ a (2×2) supercell and a $9 \times 9 \times 1$ **k**-point mesh. All results shown here are calculated with one carbon-containing species per (2×2) cell, *i.e.* a coverage of 0.25 ML of carbon, to match as closely as possible experimental carbon coverages. The adsorption energy of CH_2 and CH at both hcp sites and fcc sites was converged to 0.02 eV with respect to the basis set, **k**-grid mesh, the total number of layers, and the relaxed number of layers. Our convergence tests show that seven layers or more are necessary to obtain adsorption convergence to 0.02 eV (see more details in the Supporting Information). Vibrational frequencies and the free energies are calculated in the harmonic approximation [38] with all Ru layers fixed.

For the (2×2) supercell of Ru(0001) surface, we calculated all possible configurations of $CH_x + yH$ ($x = 1, 2, 3$ and $y = 1–3$) with all CH_x and H located at fcc or hcp hollow sites. To check whether there is a thermodynamically stable $CH_2 + nH$ ($n = 0–3$) phase, we compare calculated Gibbs free energies of adsorption (ΔG) for different adsorbate configurations defined following prior workers [39,40]:

$$\Delta G(T, p_{H_2}) = E_{CH_x+yH/slab} - E_{C/slab} + F^{vib}(T) - (x+y)\mu_H(T, p_{H_2}) \quad (3)$$

where the first and second terms are the total energy of the Ru slab with adsorbed CH_x+yH and of the slab with only C atom as adsorbate, the third term is the Helmholtz vibrational free energy of the CH_x+yH@Ru(0001) system in the harmonic approximation, and the last term is the chemical potential of hydrogen as a function of temperature T and partial pressure p_{H_2}:

$$\mu_H(T, p_{H_2}) = \frac{1}{2}(E^{total}_{H_2} + E^{ZPE}_{H_2}) + \Delta\mu_H(T, p^0_{H_2}) + \frac{1}{2}k_B T \ln\left(\frac{p_{H_2}}{p^0_{H_2}}\right) \quad (4)$$

where $\Delta\mu_H(T, p^0_{H_2})$ is obtained from partition function based on DFT calculations, $p^0_{H_2}$=1 atm.

Transition states for different possible pathways of CH_2 dissociation with and without hydrogen blocking the dissociation path were obtained using the string method [41] with a climbing image. This approach samples the configurational space between initial and final state with an intrinsically parametrized string and has been shown to be accurate and stable for the identification of transition states in similar systems [42].

The free energy pathways were calculated by adding harmonic vibrational free energy to the total energy for each structure. For the transition states, the vibrational mode corresponding to the reaction coordinate does not contribute to the free energy. For the H_2 molecule in the gas phase, also translational and rotational contributions are added to the free energy (*i.e.*, the free energy of the H_2 molecule is $2\mu_H$).

3. Experimental results

The results for samples created by dosing for 30 min on Ru(0001) at T_{Ru} = 250 K are shown in Fig. 2. The coverage of the surface is between 0.15–0.2 ML of carbon. As is clear by inspection, such a preparation produces a sample whose spectral response is dominated by a single resonance whose intensity decreases on heating (as shown in the Supporting Information, it vanishes for $T_{Ru} > 300$ K during annealing). Fitting the data with the line shape model from Eq. (1) suggests that this resonance has a center frequency of 2940 cm^{-1} before heating, and that both its center frequency and line width change slightly as peak amplitude decreases. To assign this spectral feature, we turn to prior work.

Tebbe et al. [43] found, after dosing Ru(0001) with either CH_2N_2 or C_2H_4 at low temperatures in UHV, a resonance also centered at 2940 cm^{-1} in their HREELs spectrum that they assigned to the ν_s of CH_2. In contrast Zhou and coworkers, after preparing a CH_2 containing Ru(0001) surface via dosing of CH_3I at low temperatures, report a ν_s of CH_2 of 2920 cm^{-1} [14]. Our data are consistent with a scenario in which the frequency of the ν_s of CH_2 is a function of the presence of coadsorbed I but addressing such effects is clearly beyond the scope of this work. While reported CH_2 frequencies seem to be a function of coadsorbate number and type, the thermal stability of the spectral feature assigned to CH_2, *i.e.* 190–290 K, appears independent of preparation method [14–16]. As is shown below, the mode we observe is stable over this temperature range. Finally, we note that in this temperature range, but at higher carbon coverages (≈0.37 ML relative to our 0.18), several prior studies have identified the presence of CCH_3 argued to have formed via the reaction $CH_2 + CH_2 \rightarrow CCH_3 + H$ [14–16]. In control experiments at higher carbon coverages (data and further discussion in the Supporting Information), we observed an additional spectral feature at the frequency of CCH_3 (previously unambiguously identified during the thermal decomposition of ethylene on Ru(0001) [44]). Given the frequency of the mode observed at 0.18 ML of carbon, its thermal stability and the appearance of CCH_3 at higher carbon coverages it thus seems clear that the resonance shown in Fig. 2 is the ν_s of CH_2.

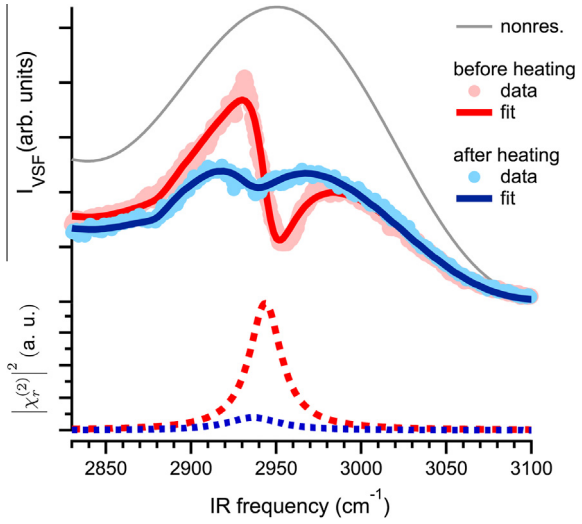

Fig. 2. (upper panel) Measured I_{VSF} before (red dots) and after (blue dots) sample annealing to 273 K. Solid lines are fits to the data using the lineshape model in Eq. (1). Gray line is the measured signal off of the bare Ru(0001) crystal, and reflects the frequency dependence of the incident IR pulse. (lower panel) Resonant intensities extracted from the fits to the data shown in the upper panel. (For interpretation of the references to colour in this figure legend, the reader is referred to the web version of this article.)

As is apparent from Fig. 2, moderate heating of the sample leads to a pronounced decay in the CH_2 resonance intensity. While perhaps clear from our experimental protocol (see Fig. 1), it is worth emphasizing that this temperature induced loss of the CH_2 spectral response is irreversible: cooling the sample does not lead to a reappearance. To quantify the loss of resonance intensity, we performed a series of experiments following the scheme shown in Fig. 1. This approach results in pairs of spectra similar to those in Fig. 2 as a function of annealing temperature. As is clear from Eq. (2), this decrease in CH_2 resonant intensity can be related to decrease in surface CH_2 concentration by subtracting the square root of the resonant intensities measured before and after sample heating.

To quantify this further, we need insight into the mechanism by which surface CH_2 population decreases. As discussed in more detail in the Supporting Information, experiments in which we dose methane at still higher temperatures and different carbon

coverages strongly suggest that the dominant mechanism of CH_2 loss with increasing sample temperature is the reaction $CH_2 \rightarrow CH + H$. This is consistent with prior experimental work dosing Ru(0001) with other CH_x containing compounds [15,16,14], as well as prior computational results [17]. Given this loss channel, and assuming the reaction is first order in surface CH_2 concentration (assuming the reaction is zeroeth order yields quantitatively similar results, see Supporting Information) we write,

$$\frac{\partial[CH_2]}{\partial t} = -k[CH_2] = -A \cdot e^{\frac{-E_a}{RT}}[CH_2] \quad (5)$$

in which $[CH_2]$ is the surface concentration of CH_2, A is the pre-exponential factor, R the gas constant, T temperature and E_a the activation energy of dissociation. Rewriting Eq. (5) and assuming that the pre-exponential factor is temperature-independent (see Supporting Information for justification) gives,

$$\ln\left(\frac{\Delta[CH_2]}{[CH_2]}\right) = -\frac{E_a}{RT} + \text{const} \quad (6)$$

Taking the denominator on the left-hand side of Eq. (6) as the average of the surface CH_2 concentration before and after heating allows us to straightforwardly fit this expression to the data shown in Fig. 3 and extract that for the reaction $CH_2 \rightarrow CH + H$ $E_a = 65 \pm 6$ kJ/mol. Note that, as mentioned above, within our experimental set up this loss of CH_2 is irreversible so this extracted E_a reflects only the barrier for the $CH_2 \rightarrow CH + H$ reaction.

While the barrier for this reaction has not been observed experimentally previously, it has been calculated using electronic-structure-based approaches and found to be 16 kJ/mol [18,17]. This experiment/computation disagreement implies that the systems considered in each work differ in a manner which influences the underlying potential energy surface for the $CH_2 \rightarrow CH + H$ reaction. Prior work in other catalytic systems has highlighted the role of *carbon* and *hydrogen* surface coverage in controlling similar surface chemistry [45]. As mentioned in the methods section, the dosing protocol we followed with our MBS creates coadsorbed *hydrogen atoms* in addition to those originating from CH_4 molecules that dissociatively adsorb. To understand the possible influence of this coadsorbed hydrogen on the kinetics and thermodynamics of the $CH_2 \rightarrow CH + H$ reaction, we turn to theory.

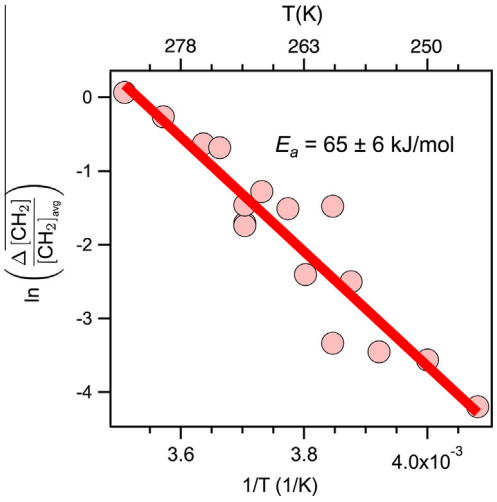

Fig. 3. Change in surface population of CH_2 radicals, divided by average population, as a function of annealing temperature.

4. Theoretical results

Coadsorbed hydrogen may, most simply, effect the $CH_2 \rightarrow CH + H$ reaction by changing the free energy of the reactant(s): *e.g.* changing the energetically preferred adsorption site of CH_2. We explore this dependence by calculating the difference in adsorption energy of CH_2, and H atoms, between hcp and fcc sites on Ru(0001) (other possible sites lead to dramatically less favorable adsorption energies, see Supporting Information for further discussion). The adsorption energy of a single CH_2 molecule at the hcp site of the Ru(0001) surface is 17.0 kJ/mol more favorable than adsorption at the fcc site (see structure (i) in Fig. 5). However, the situation changes as the hydrogen coverage is increased: adding one H atom per (2×2) surface unit cell significantly decreases the difference between hcp and fcc adsorption energies for the $CH_2 + H$ system. Interestingly, the preferred site changes from hcp to fcc when two H atoms are coadsorbed (see Table 1). Addition of the third coadsorbed H atom further stabilizes $CH_2 + 3H$ at the fcc versus hcp sites. Evidently, coadsorbed hydrogen dramatically changes the energetically favorable adsorption site of the CH_2 reactant.

Clearly, however, to fully understand the effect of coadsorbed H on the $CH_2 \rightarrow CH + H$ reaction, we need to understand the energies and barrier(s) along the reaction coordinate. To do so, we next analyze the total energy changes along the minimum energy paths for the reactions $CH_2 + xH \rightarrow CH + (x+1)H$ ($x = 0$–3). The results of this analysis are shown in Table 2. CH_2 dissociation is found to be energetically favored for $x = 0$–2. For $x = 0$ our all-electron PBE calculations give a dissociation barrier (11.2 kJ/mol), similar to the result of Van Santen et al. (16 kJ/mol) [17]. However, there is a striking difference between the dissociation barrier at the highest coverage considered (3 coadsorbed H atoms per unit cell) and the barrier at the lower coverages (0–2 H atoms per unit cell). For the high coverage, we consider two different dissociation pathways: one with the hydrogen coming from CH_2 staying at the surface, and one with hydrogen desorbing as H_2. The corresponding calculated reaction barriers are 61.8 kJ/mol and 95.6 kJ/mol.

Table 1
Energetically preferred adsorption site for CH_2 and H atoms on a (2×2) surface supercell of Ru(0001) as a function of the number of H atoms. The last two columns show the energy differences between most stable configurations of CH_2 at hcp sites and at fcc sites for a given number of hydrogen atoms, with and without ZPE.

CH_2	H	H	H	$E_{hcp} - E_{fcc}$ (kJ/mol)	$E_{hcp} - E_{fcc} + \Delta ZPE$ (kJ/mol)
hcp	–	–	–	−17.0	−17.4
hcp	hcp	–	–	−4.2	−5.6
fcc	fcc	fcc	–	4.8	3.2
fcc	fcc	fcc	fcc	11.0	13.3

Table 2
Calculated reaction barrier (middle column) and reaction energy (right column) for CH_2 dissociation with different numbers of H atoms on a (2×2) supercell of Ru(0001). E_{IS}, E_{TS}, E_{FS} are total energies of initial state, transition state, and final state, respectively. The final state of reaction $CH_2 + 3H \rightarrow (CH + 4H)$ is shown in Fig. 5, panel (e). For each stoichiometry, the most stable configuration of the initial state is considered (see Supporting Information for further details).

Reaction	$E_{TS} - E_{IS}$ (kJ/mol)	$E_{FS} - E_{IS}$ (kJ/mol)
$CH_2 \rightarrow CH + H$	11.2	−49.0
$CH_2 + H \rightarrow CH + 2H$	10.8	−35.0
$CH_2 + 2H \rightarrow CH + 3H$	12.4	−39.5
$CH_2 + 3H \rightarrow CH + 4H$	61.8	53.1
$CH_2 + 3H \rightarrow CH + 2H + H_{2,gas}$	95.6	51.8

Given the DFT energetics, we next calculated harmonic vibrational frequencies for reactants, products and all intermediates to obtain free energy profiles at the experimental conditions ($T = 300$ K and $p_{H_2} = 10^{-10}$ atm) for the reactions $CH_2 \rightarrow CH + H$ (low H coverage) and $CH_2 + 3H \rightarrow CH + 4H$ or $CH_2 + 3H \rightarrow CH + 2H + H_2$(gas) (both high H coverage). The results are summarized in Fig. 4. For an adsorbed CH_2 molecule in the absence of coadsorbed hydrogen, vibrational contributions lower the calculated barrier from 11.2 to 4.0 kJ/mol and the ΔG of reaction by a similar amount (Fig. 4, inset). Of the reactions, we consider at high H coverage, $CH_2 + 3H \rightarrow CH + 4H$ (*i.e.* (a) → (b) → (c) → (d) → (e) see Fig. 5) has a lower free energy barrier (47.4 kJ/mol versus 88.4 kJ/mol), but it is endergonic (*i.e.* $\Delta G > 0$), and its reverse reaction has a low free energy barrier (7.8 kJ/mol). As a consequence, this reaction cannot be the irreversible channel for CH_2 conversion to CH observed in experiment. In contrast, the reaction $CH_2 + 3H \rightarrow CH + 2H + H_2$(gas) (*i.e.* (a) → (b) → (c) → (f) → (g)) has a higher barrier, but it is exergonic (although endothermic) and leads eventually to the irreversible conversion of CH_2 to CH at higher temperatures. During this process, the hydrogen molecule leaves the surface via a physisorbed precursor state (not shown). Note

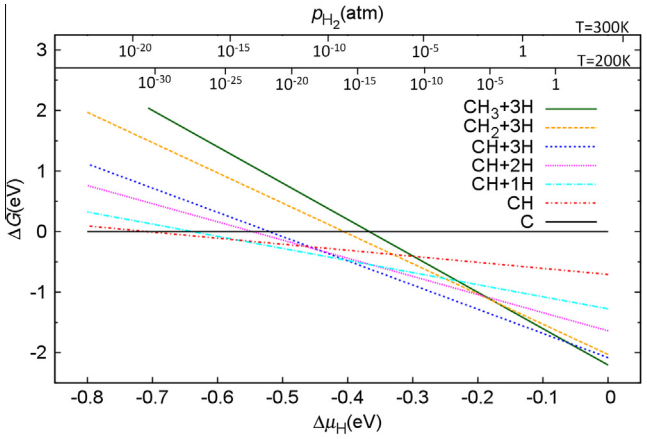

Fig. 6. Gibbs free energy of adsorption for $CH_x + yH$ ($x + y = 0$–6) configurations on a (2×2) Ru(0001) surface model, calculated using Eq. (3) (F^{vib}(300 K) is used; the maximum difference between F^{vib} (300 K) and F^{vib} (200 K) is less than 0.02 eV) as a function of the hydrogen chemical potential defined by Eq. (4). For clarity, only the most stable adsorption configuration for each value of $x + y$ is shown. All calculated structures and corresponding energies are given in the Supporting Information.

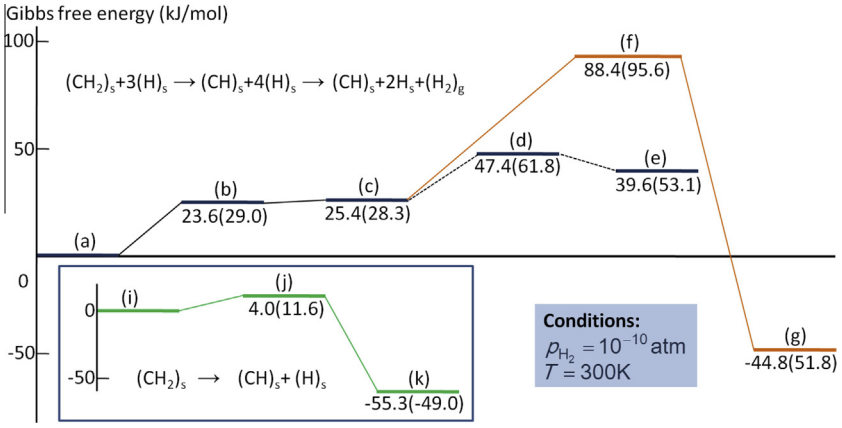

Fig. 4. Calculated free-energy profile for dissociation of $CH_2 + 3H$ on a Ru(0001) (2×2) surface supercell at $T = 300$ K, $p_{H_2} = 10^{-10}$ atm. Total energy differences are shown in parenthesis. The structures are labeled according to Fig. 5. The inset shows the dissociation pathway for a CH_2 molecule in the absence of coadsorbed hydrogen for the same (2×2) unit cell.

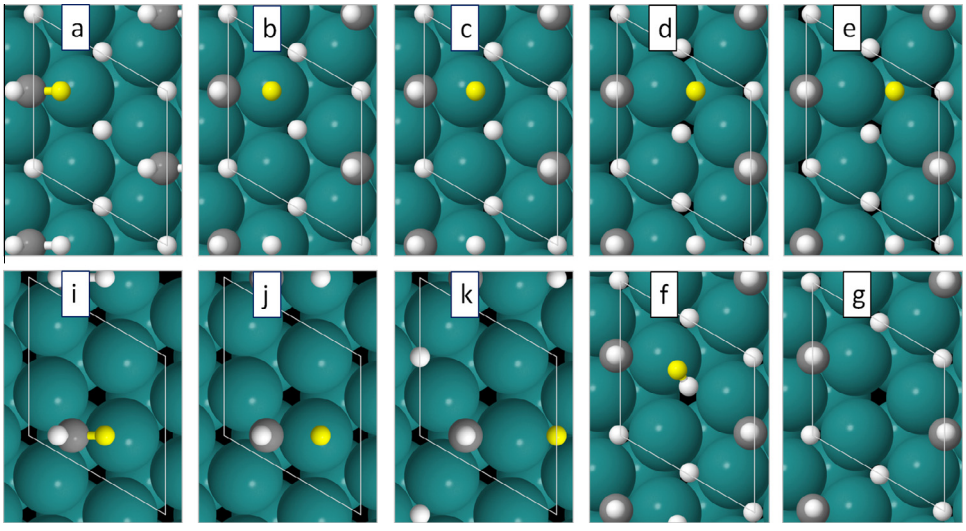

Fig. 5. Calculated local-minimum and transition-state structures for CH_2 dissociation. Blue, grey, white and black spheres are ruthenium, carbon, hydrogen, and unfilled sites respectively. The hydrogen atom coming from CH_2 is highlighted in yellow. (For interpretation of the references to colour in this figure legend, the reader is referred to the web version of this article.)

that we also tried to find another (direct) minimum energy pathway connecting states (e) and (f) or (g), but the indirect pathway (e) → (d) → (c) → (f) → (g) was always recovered.

While it is thus clear that both the kinetics and thermodynamics of the $CH_2 \rightarrow CH$ conversion are dramatically different in the presence of 3 coadsorbed hydrogen, it is still unclear whether CH_2 + 3H on Ru(0001) is thermodynamically stable. To clarify this point, we analyzed the relative thermodynamic stability of all $CH_x + yH$ $(x + y = 0–6)$ adsorption configurations for the (2×2) surface unit cell of Ru(0001). By calculating the adsorption free energy of all possible species as a function of the chemical potential of hydrogen (employing Eq. (3)), we arrive at the phase diagram for one carbon species shown in Fig. 6. Clearly, three coadsorbed hydrogen atoms per CH_2 molecule at the considered carbon coverage is not thermodynamically stable configuration at the relevant conditions.

5. Discussion

Our computational results clearly demonstrate that, in the presence of three coadsorbed H atoms, the kinetics and thermodynamics of the $CH_2 \rightarrow CH$ conversion change dramatically. To understand the relevance of these results for our experimental findings, we next explore the question of how much atomic H might be expected to be on our experimentally generated Ru(0001) surface in more detail.

Prior TPD studies of hydrocarbon adsorption on Ru(0001) have shown that atomic hydrogen, at sub-monolayer surface converges, recombinatively desorbs from this surface only at temperatures >300 K [19]. Because we both prepare our samples below 300 K and the temperature window we probe in experiment is below 300 K, we expect that hydrogen does not desorb from our surface under our experimental conditions.

Three ways of adding atomic H to the surface seem possible. Firstly, because we generate our CH_2 radicals from CH_4, and because our observed CH_2 spectral response disappears below 300 K, we expect that the 2 hydrogen atoms originating from each adsorbed CH_4 molecule should remain on the surface in our temperature window of interest. Secondly, as noted in the Methods section, prior MBS studies employing CH_4 seeded in He in setups similar to ours have found partial dehydrogenation of CH_4 in the nozzle above 860 K [23] (we employed a T_{nozzle} of 980 K). While we did not quantify this hydrogen flux in our system, it is clear that similar dehydrogenation happens in our nozzles (over timescales of weeks they become clogged with carbon deposits). Because the sticking coefficient of hydrogen on Ru(0001) in our experimental temperature window is high relative to methane (10^{-1} versus 10^{-6} [sticking probability/molecule]), extremely small amounts of nozzle dehydrogenation are sufficient to generate substantial numbers of additional hydrogen atoms on the Ru(0001) surface. Thirdly, as noted in the Methods section, the CH_4:He mixture in our MBS contains trace amounts of H_2. Both effects suggest we may have atomic H on the surface in addition to that which originates from the dissociation of CH_4. As discussed in detail in the Supporting Information, quantitative estimates of both effects strongly suggest we probe dehydrogenation in the CH_2 + 3H system. Thus, the dramatically higher barrier for $CH_2 \rightarrow CH$ conversion, relative to both prior calculations can be straightforwardly understood as an H atom surface coverage effect.

As described above, CH_2 + 3H is predicted to be thermodynamically unstable. This would suggest that, if we probe CH_2 to CH conversion from the CH_2 + 3H state, our reactants are not at equilibrium with gas-phase hydrogen at any chemical potential. Such a non-equilibrium state is consistent with our method of gas dosing, relatively low sample temperature and the relatively high sticking coefficient of H_2. However, more experiments (particularly investigating the dependence of this inferred hydrogen saturation on nozzle and sample temperature) are necessary to completely clarify this issue.

Our experimental and theoretical results suggest that CH_2 is converted to CH on Ru(0001) at temperatures below 300 K. However, a clear spectral response of CH is detected in our experiments only at temperatures above 300 K. This could be explained by damping the spectral intensity of the CH stretching mode by co-adsorbed hydrogen. As mentioned above, a mode's hyperpolarizability is proportional to the product of the transition dipole and polarizability squared. Because polarizability is generally less sensitive to local environment than the transition dipole, we have computed the squared derivative of the dipole moment component along the surface normal for the 2×2 surface unit cell with different number of H atoms (0–3), as a measure of the signal intensity. The dipole moment derivative is calculated along the harmonic vibrational normal mode corresponding to the CH stretch (the normal mode is calculated keeping all Ru atoms in the unit cell fixed, and all adsorbed species are allowed to move; only phonon Γ-point is considered). We find that the intensity of the CH vibration is dramatically *reduced* when hydrogen atoms co-adsorb with CH. Relative to a single adsorbed CH molecule, the squares of the dipole moment derivative for adsorbed (CH+H):(CH+2H):(CH+3H) are 0.005:0.031:0.006 for CH at fcc site, and 0.032:0.014:0.046 for CH at hcp site. For CH_2, the higher H coverage *increases* the IR absorption intensity for the CH stretching vibrational mode of adsorbed CH_2: it is 12.9 times higher for CH_2+3H when CH_2 is at the fcc site, and 2.7 times higher when CH_2 is at the hcp site. In all cases (both for CH and CH_2), the intensities are calculated for the energetically most stable (according to PBE) configuration of the co-adsorbed hydrogen. Thus, although the exact mechanism behind the effects of H coverage on the spectrum is not understood, our PBE calculations explain why we do not observe a spectroscopic signature of CH at the lower temperatures.

Effects of non-equilibrium hydrogen saturation on hydrocarbon chemistry at the Ru(0001) surface have not been described in samples prepared via molecular beam sources previously. Nevertheless, there are hints of the influence of coadsorbed hydrogen on hydrocarbon stability for samples prepared at high pressure and temperature in the presence of gas-phase H_2. Goodman and coworkers [46] previously showed that dosing a Ru(0001) surface with high pressures of CO and H_2, and subsequently cooling and transporting the sample to UHV for analysis using EELS, produces a notable loss feature at 1395 cm^{-1}, *i.e.*, the frequency of the H–C–H scissor mode. This loss feature disappears on annealing of the sample to 500 K in UHV. Based on our results and the known thermal stability of H on Ru(0001) [19], this observation can be most easily rationalized by the desorption of hydrogen, which recombinatively desorbs almost completely upon annealing to 500 K in UHV, dramatically destabilizing the adsorbed CH_2.

Finally, our results show that the conversion of CH_2 to CH on Ru(0001) must be kinetically controlled, since adsorbed CH species are thermodynamically stable at realistic conditions. This clarifies why CH_2 and/or CH_3 were observed after decomposition of hydrocarbons, but only CH could be found when hydrogenating atomic carbon at the Ru surface [47]. Prior work on Fischer–Tropsch synthesis has argued for the importance of CH or C as the C_1 building block of longer chain growth, based at least in part on calculations assuming the absence of abundant, non-equilibrium, coadsorbed hydrogen, and on experiments that do not quantify the presence of surface coadsorbed H. Our results suggest that considering such surface H leads to re-evaluation of the stability of CH_2 relative to other CH_x surface radicals and support the idea of the enhanced role for this species in the Fischer–Tropsch process [48]. Clearly, more detailed *in situ* studies are necessary to further understand

elementary steps of technologically important processes of hydrocarbon conversion on metal surfaces.

6. Summary and conclusions

By using a molecular beam source to dose methane in UHV, we have created a Ru(0001) surface dominated by surface-bound CH_2 that is stable at low temperatures and can be converted to CH at high temperatures. The temperature dependence of the rate of CH_2 to CH conversion, quantified using the laser-based vibrational sum frequency spectroscopy, allows us to extract an experimental estimate for the activation energy of this process. The resulting barrier for the $CH_2 \rightarrow CH + H$ reaction of 65 kJ/mol is (four times) larger than previous computational reports [17,18]. Computational results presented here clarify that the origin of this experimental result is likely the presence of *additional* coadsorbed hydrogen blocking surface adsorption sites. Assuming CH_2 is converted to CH via the reaction $CH_2 + 3H \rightarrow CH_2 + 2H + H_2(g)$, the calculated barrier is 88.4 kJ/mol, and the reaction is essentially irreversible, both characteristics consistent with experiment. Computation further clarifies that the stabilized CH_2 we observe requires H_2 in the gas phase to not be in equilibrium with adsorbed H. CH_2 is not thermodynamically favored at any realistic value of the chemical potential of gas-phase hydrogen.

Several decades of work have investigated the molecular-level mechanisms of the Fischer–Tropsch process [7,8,6,48–50]. Much debate has centered on the mechanism by which chains grow: by direct insertion of CO, addition of CH, CH_2 or C. Based on calculations either at equilibrium, or in the absence of our coadsorbed hydrogen, the importance of CH_2 has been minimized. Our work here suggests that such conclusions should be revisited employing careful *in situ* experiments as a function of coadsorbed H.

More generally, while the effects of carbon coverage on the thermal stability of hydrocarbon fragments have received attention in prior work [45], the effect of non-equilibrium concentrations of surface hydrogen, has been much less appreciated. This study suggests that such effects can dramatically change the thermodynamics and kinetics of hydrocarbon chemistry at catalytic surfaces. While we create the non-equilibrium effects using a molecular beam source and relatively low sample temperatures, there is evidence from past studies that such effects also likely occur in samples at elevated temperatures and pressures, suggesting that the effect we describe has large potential relevance.

Acknowledgments

SVL thanks the Cluster of Excellence UniCat for support. All authors gratefully acknowledge support of the Max Planck Society.

Appendix A. Supplementary material

Supplementary data associated with this article can be found, in the online version, at http://dx.doi.org/10.1016/j.jcat.2014.09.023.

References

[1] S.-G. Wang, D.-B. Cao, Y.-W. Li, J. Wang, H. Jiao, Surf. Sci. 600 (2006) 3226–3234.
[2] M.-C. Wu, D.W. Goodman, Surf. Sci. Lett. 306 (1994) 529–533.
[3] P. Lenz-Solomun, M.-C. Wu, D.W. Goodman, Catal. Lett. 25 (1994) 75–86.
[4] M.-C. Wu, D.W. Goodman, J. Am. Chem. Soc. 116 (1994) 1364–1371.
[5] J.H. Larsen, P.M. Holmblad, I. Chorkendorff, J. Chem. Phys. 110 (1999) 2637–2642.
[6] R.A. van Santen, I.M. Ciobîcă, E. van Steen, M.M. Ghouri, Adv. Catal. 54 (2011) 127–187.
[7] R.C. Brady III, R. Pettit, J. Am. Chem. Soc. 103 (1981) 1287–1289.
[8] R.C. Brady III, R. Pettit, J. Am. Chem. Soc. 102 (1980) 6181–6182.
[9] R.C. Egeberg, S. Ullmann, I. Alstrup, C.B. Mullins, I. Chorkendorff, Surf. Sci. 497 (2002) 183–193.
[10] G. Jones, J.G. Jakobsen, S.S. Shim, J. Kleisa, M.P. Andersson, J. Rossmeisl, F. Abild-Pedersen, T. Bligaard, S. Helveg, B. Hinnemann, J.R. Rostrup-Nielsen, I. Chorkendorff, J. Sehested, J.K. Norskov, J. Catal. 259 (2008) 147–160.
[11] H.L. Abbott, I. Harrison, J. Catal. 254 (2008) 27–38.
[12] M.-C. Wu, P. Lenz-Solomun, D.W. Goodman, J. Vac. Sci. Technol. A 12 (1994) 2205–2209.
[13] T.V. Choudhary, D.W. Goodman, Top. Catal. 20 (2002) 35–42.
[14] Y. Zhou, M.A. Henderson, W.M. Feng, J.M. White, Surf. Sci. 224 (1989) 386–406.
[15] A. Kis, J. Kiss, F. Solymosi, Surf. Sci. 459 (2000) 149–160.
[16] A. Kis, K.C. Smith, J. Kiss, F. Solymosi, Surf. Sci. 460 (2000) 190–202.
[17] I.M. Ciobîcă, F. Frechard, R.A. van Santen, A.W. Kleyn, J. Hafner, J. Phys. Chem. B 104 (2000) 3364–3369.
[18] B. Xing, X.-Y. Pang, G.-C. Wang, J. Catal. 282 (2011) 74–82.
[19] M.M. Hills, J.E. Parmeter, C.B. Mullins, W.H. Weinberg, J. Am. Chem. Soc. 108 (1986) 3554–3562.
[20] K. Reuter, C. Stampf, M. Scheffler, in: Handbook of Materials Modeling, Springer, Netherlands, 2005, pp. 149–194.
[21] S.T. Ceyer, Annu. Rev. Phys. Chem. 39 (1988) 479–510.
[22] P.R. McCabe, L.B.F. Juurlink, A.L. Utz, Rev. Sci. Instr. 71 (2000) 42–53.
[23] M.B. Lee, Q.Y. Yang, S.T. Ceyer, J. Chem. Phys. 87 (1987) 2724–2740.
[24] S. Funk, M. Bonn, D.N. Denzler, C. Hess, M. Wolf, G. Ertl, J. Chem. Phys. 112 (2000).
[25] Y.R. Shen, Nature 337 (1989) 519–525.
[26] Y.R. Shen, Proc. Natl. Acad. Sci. USA 93 (1996) 12104–12111.
[27] G.L. Richmond, Annu. Rev. Phys. Chem. 52 (2001) 357–389.
[28] G.L. Richmond, Chem. Rev. 102 (2002) 2693–2724.
[29] P. Magnan, Nucl. Instrum. Methods A 504 (2003) 199–212.
[30] C. Hess, M. Bonn, S. Funk, M. Wolf, Chem. Phys. Lett. 325 (2000) 139–145.
[31] H. Dietrich, P. Geng, K. Jacobi, G. Ertl, J. Chem. Phys. 104 (1996) 375–381.
[32] M.A. Barteau, J.Q. Broughton, D. Menzel, Appl. Surf. Sci. 19 (1984) 92–115.
[33] P. Hohenberg, W. Kohn, Phys. Rev. 136 (1964) 864–871.
[34] R.G. Parr, W. Yang, Oxford University Press, 1989.
[35] V. Blum, R. Gehrke, F. Hanke, P. Havu, V. Havu, X. Ren, K. Reuter, M. Scheffler, Comp. Phys. Commun. 180 (2009) 2175–2196.
[36] J.P. Perdew, K. Burke, M. Ernzerhof, Phys. Rev. Lett. 77 (1996) 3865–3868.
[37] V.G. Ruiz, W. Liu, Z. Egbert, M. Scheffler, A. Tkatchenko, Phys. Rev. Lett. 108 (2012) 146103.
[38] B.A. Hess Jr, L.J. Schaad, P. Carsky, R. Zahradnik, Chem. Rev. 86 (1986). 709–130.
[39] M. Scheffler, J. Dabrowski, Phil. Mag. A 58 (1988) 107–121.
[40] K. Reuter, M. Scheffler, Phys. Rev. B 65 (2002) 045407.
[41] W. E, W. Ren, E. Vanden-Eijnden, Phys. Rev. B 66 (2002) 052301.
[42] W. E, W. Ren, E. Vanden-Eijnden, J. Chem. Phys. 126 (2007) 164103.
[43] P.M. George, N.R. Avery, W.H. Weinberg, F.N. Tebbe, J. Am. Chem. Soc. 105 (1983) 1393–1394.
[44] I.A. Ransley, L.M. Ilharco, J.E. Bateman, B.H. Sakakini, J.C. Vickerman, M.A. Chesters, Surf. Sci. 298 (1993) 187–194.
[45] M. Neurock, V. Pallassana, R.A. van Santen, J. Am. Chem. Soc. 122 (2000) 1150–1153.
[46] M.-C. Wu, D.W. Goodman, G.W. Zajac, Catal. Lett. 24 (1994) 23–30.
[47] T.K. Shimizu, A. Mugarza, J.I. Cerdá, M. Salmeron, J. Chem. Phys. 129 (2008) 244103.
[48] I.M. Ciobîcă, G.J. Kramera, Q. Ge, M. Neurock, R.A. van Santen, J. Catal. 212 (2002) 136–144.
[49] Z.-P. Liu, P. Hu, J. Am. Chem. Soc. 124 (2002) 11568–11569.
[50] J. Cheng, P. Hu, P. Ellis, S. French, G. Kelly, C.M. Lok, Top. Catal. 53 (2010) 326–337.